THE ASTROPHYSICAL JOURNAL, 442:523–537, 1995 April 1

A MULTIPARAMETRIC ANALYSIS OF THE *EINSTEIN* SAMPLE OF EARLY-TYPE GALAXIES. II. GALAXY FORMATION HISTORY AND PROPERTIES OF THE INTERSTELLAR MEDIUM

PAUL B. ESKRIDGE[1,2] AND GIUSEPPINA FABBIANO[3]
Harvard-Smithsonian Center for Astrophysics, 60 Garden Street, Cambridge, MA 02138
AND
DONG-WOO KIM[4]
Harvard-Smithsonian Center for Astrophysics; and Department of Astronomy and Space Science, Chungnam National University, Taejon, 305-764, South Korea
Received 1994 July 22; accepted 1994 October 12

ABSTRACT

We have conducted bivariate and multivariate statistical analysis of data measuring the integrated luminosity, shape, and potential depth of the *Einstein* sample of early-type galaxies (presented by Fabbiano et al. 1992). We find significant correlations between the X-ray properties and the axial ratios (a/b) of our sample, such that the roundest systems tend to have the highest L_X and L_X/L_B. The most radio-loud objects are also the roundest. We confirm the assertion of Bender et al. (1989) that galaxies with high L_X are boxy (have negative a_4). Both a/b and a_4 are correlated with L_B, but not with *IRAS* 12 μm and 100 μm luminosities. There are strong correlations between L_X, Mg_2, and σ_v in the sense that those systems with the deepest potential wells have the highest L_X and Mg_2. Thus the depth of the potential well appears to govern both the ability to retain an ISM at the present epoch and to retain the enriched ejecta of early star formation bursts. Both L_X/L_B and L_6 (the 6 cm radio luminosity) show threshold effects with σ_v, exhibiting sharp increases at $\log(\sigma_v) \approx 2.2$. Finally, there is clearly an interrelationship between the various stellar and structural parameters: The scatter in the bivariate relationships between the shape parameters (a/b and a_4) and the depth parameter (σ_v) is a function of abundance in the sense that, for a given a_4 or a/b, the systems with the highest σ_v also have the highest Mg_2. Furthermore, for a constant σ_v, disky galaxies tend to have higher Mg_2 than boxy ones. Alternatively, for a given abundance, boxy ellipticals tend to be more massive than disky ellipticals. One possibility is that early-type galaxies of a given mass, originating from mergers (boxy ellipticals), have *lower* abundances than "primordial" (disky) early-type galaxies. Another is that disky inner isophotes are due not to primordial dissipational collapse, but to either the self-gravitating inner disks of captured spirals or the dissipational collapse of new disk structures from the premerger ISM. The high measured nuclear Mg_2 values would thus be due to enrichment from secondary bursts of star formation triggered by the merging event.

Subject headings: galaxies: elliptical and lenticular, cD — galaxies: ISM — galaxies: structure — X-rays: galaxies

1. INTRODUCTION

The connection between the structural and stellar properties of galaxies and the nature of their interstellar medium (ISM) was first discussed by Spitzer (1954). The basic situation, as it was understood ~35 years ago, was laid out by Sandage (1961). Our ability to observe, and thus our understanding of, the ISM has increased enormously since then. Current observational techniques allow us to collect data on the solid phase of the ISM (dust grains), as well as gas phases ranging from cold molecular cloud cores ($T \sim 10$ K, $n \sim 10^6$ cm^{-3}) to X-ray–emitting gas ($T \sim 10^{6-7}$ K, $n \gtrsim 0.1$ cm^{-3}). Our understanding of the relationships between ISM properties and the structural and stellar properties of galaxies is thus undergoing a concomitant rapid development.

Early-type (E and S0) galaxies, once considered devoid of intestellar gas, are now known to possess rich and complex ISM. Although many early-type galaxies exhibit the ISM tracers more traditionally associated with late-type galaxies (e.g., Huchtmeier & Richter 1989 and Eder, Giovanelli, & Haynes 1991 for H I; Sage & Wrobel 1989 and Thronson et al., 1989 for CO; Goudfrooij et al. 1994 for Hα; Knapp et al. 1989 for FIR), X-ray observations, beginning with the *Einstein Observatory* (Giacconi et al. 1979) have demonstrated that the ISM in luminous early-type galaxies is typically dominated by a hot ISM (see Fabbiano 1989 and references therein).

In the previous paper of this series (Eskridge, Fabbiano, & Kim 1995, hereafter P1), we presented an analysis of the ISM properties of the *Einstein* sample of early-type galaxies (Fabbiano, Kim, & Trinchieri 1992, hereafter P0). The major results of P1 are as follows: In agreement with previous studies (see Fabbiano 1989 and references therein), we find a strong correlation between L_B and L_X, with a power-law slope of 1.8 ± 0.1. However, this is actually a combination of a slope 1 relation for the fainter galaxies [$\log(L_X) \leq 40.5$] and a slope 2 relation for the more luminous galaxies. This result is consistent with previous work indicating that X-ray–faint early-type galaxies do not retain any significant quantities of hot ISM (Trinchieri & Fabbiano 1985; Fabbiano, Gioia, & Trinchieri 1989, hereafter FGT). In this case, their X-ray emission should be dominated by the integrated output of discrete sources similar to those found in the bulge of M31 (van Speybroeck et al. 1979). The X-ray emission from more distant spiral bulges is

[1] Current address: Department of Physics and Astronomy, University of Alabama, Tuscaloosa, AL 35487.
[2] paul@hera.astr.ua.edu.
[3] pepi@cfa.harvard.edu.
[4] kim@cfa.harvard.edu.

well modeled by a composite of such sources (Fabbiano, Gioia, & Trinchieri 1988). These results are also supported by differences found between the X-ray spectra of X-ray–bright and X-ray–faint E and S0 galaxies, suggesting the presence of stellar emission in the X-ray–faint objects (Kim, Fabbiano, & Trinchieri 1992b; Fabbiano, Kim, & Trinchieri 1994; Fabbiano 1994).

The mean values of the distribution functions of both L_X and L_X/L_B for the S0's are lower than those for the E's at the 2.8 σ and 3.5 σ levels, respectively. Thus, for a given stellar luminosity, the potential wells of S0's may be shallower than those of E's. The rotation of the S0 disks may be an important factor (see also Pellegrini 1994). The other differences found between E and S0 galaxies may be related to differences in their star formation histories: Our S0 sample has excess 12 μm emission compared to the E sample, when scaled by their optical luminosities. This may be due to emission from dust heated in star-forming regions in S0 disks. This interpretation is supported by the existence of a strong L_{12}-L_{100} correlation for our S0 sample that is not found for the Es and by an analysis of optical-IR colors.

We also find strong indications of a connection between galaxy ISM and nuclear activity. There are steep power-law slopes between radio luminosity and optical, X-ray properties, and FIR properties. This last point argues that the presence of a FIR-emitting ISM in early-type galaxies is coupled to their ability to generate nonthermal radio continuum, as previously argued by, e.g., Walsh et al. (1989). However, we also find that for a given L_{100}, galaxies with larger L_X/L_B tend to be stronger nonthermal radio sources, as originally suggested by Kim & Fabbiano (1990). We note that while L_B is most strongly correlated with L_6, the *total* radio luminosity (summed over a $\sim$1% bandwidth around 6 cm—see P1), both L_X and L_X/L_B are more strongly correlated with L_{6co}, the *core* radio luminosity. These points support the argument (proposed by FGT) that radio cores in early-type galaxies are fueled by the accretion of cooling flow gas from the hot ISM.

The picture that emerges from P1 connects the properties of the ISM in E and S0 galaxies to their star formation history and nuclear activity. We confirm the differences between X-ray–bright and X-ray–faint galaxies and link these differences to the relative ability to retain a hot ISM. This ability is potentially connected to galaxy morphology, but this is not a complete explanation, as both Es and S0's can be found over a very large range of L_X/L_B. However, the results of P1 suggest a link between the characteristics of the galaxy potential and the retention of a hot ISM. This is not a tautology, as other mechanisms such as ram-pressure stripping, interactions with close neighbors (e.g., White & Sarazin 1991), variation in the SN Ia rate, and overall evolutionary state of the ISM (e.g., Ciotti et al., 1991; Pellegrini & Fabbiano 1994) could also effect the L_X/L_B for galaxies of a given luminosity.

To further explore the role of the shape and depth of the galaxy potential in determining the state of the ISM in early-type galaxies and how this relates to galaxy formation mechanisms, we extend the study of P1 with a consideration of available data on the structure and stellar populations of the *Einstein* sample. The data collected in P1 (see Table 1 of P1) will be used in this paper to compare with the information relating to the structural and stellar properties of the sample. In § 2, we describe how we have built our data set for this project and review the required statistical methods. We present our analysis of the axial ratio data in § 3. The Mg_2 results are given in § 4, those for σ_v in § 5, and those for a_4 in § 6. We summarize our results and conclusions and discuss possible strategies for future research in § 7. The Appendix contains details of our statistical analysis.

2. SAMPLE CONSTRUCTION AND STATISTICAL METHODS

We have gathered information from the literature regarding the structural and chemical properties of the galaxies in our sample. Axial ratios have been taken from de Vaucouleurs et al. (1991, hereafter RC3). These are listed, for the entire sample, in Table 1 of P1. We discovered a zero-point offset between the a/b values from de Vaucouleurs, de Vaucouleurs, & Corwin (1976) and those of Faber et al. (1989, hereafter 7S). Such an offset does not exist for the RC3 values compared to the 7S values. We have therefore adopted the more extensive set of values from the RC3. The a_4 parameter, defined in Bender et al. (1989), is a measure of the amplitude of the cos (4θ) Fourier component of the deviation from ellipticity of the isophotes of early-type systems. Values of a_4 for 47 galaxies in our sample have been published by Bender et al. (1989) and Peletier et al. (1990). We have taken values of log (σ_v) (for 74 galaxies) and Mg_2 (for 73 galaxies)from 7S. All these available data are given in Table 1.

Many of our data in the X-ray, FIR, and radio are upper limits. Therefore, the use of standard statistical techniques is manifestly invalid for our project. Instead we use techniques from the field of survival analysis for both evaluating the existence of bivariate correlations amongst our data and for determining best-fit regression coefficients. These methods explicitly account for the existence of upper limits in the samples being tested, subject to regularity conditions that may or may not apply in the case of any given data sample. This last point is, of course, the standard problem in all astronomical statistical analysis. In an effort to minimize it, we use a number of different statistical tests, each with their own assumptions about the nature of the data and distribution of the upper limits, in the hopes that gross violations of the normality assumptions by our data will manifest themselves in highly discrepant results for the various statistical tests. Basic references in the astronomical literature for these methods are Feigelson & Nelson (1985), Schmitt (1985), Isobe, Feigelson, & Nelson (1986), LaValley, Isobe & Feigelson (1992), and Fiegelson & Babu (1992). Details of our particular procedures are given in P1.

As we are dealing with a multiparametric data set, it is important to investigate possible interrelationships between the various observables in our sample. A technique used in previous studies (Fabbiano et al. 1988; P1) is the partial Spearman rank method (Kendall & Stuart 1976). In brief, to apply this method, one builds a matrix of modified Spearman rank coefficients for the parameters to be tested, and then tests the correlation between subsamples of the parameters in the matrix set while holding all other variables in the matrix set constant. The major results of the partial-rank analysis are presented in the text below. The full details of our results are tabulated in Appendix A. As we do not have terribly large samples for some combinations of observables, there is some reason for concern that we may obtain correlations (or noncorrelations) from our partial-rank analysis that would not stand up if we had a truly large sample. In order to examine this possibility, we drew a number of random subsamples from our L_B-L_X-a/b and L_B-L_X-a/b-Mg_2 samples (discussed in §§ 3 and 4, below) and subjected them to partial-rank analysis. In no case did correlations appear for the subsamples that were

TABLE 1

STRUCTURAL DATA

Name	Type	log(a/b) 7S	log(a/b) RC3	Mg_2 mags	logσ_v km/sec	$a_4/a\times100$
NGC 205	-3	0.26	0.30			
NGC 221	-6	0.06	0.13	0.185	1.892	
NGC 315	-3	0.14	0.20	0.283	2.546	−0.46
NGC 499	-3	0.19	0.10	0.334	2.374	
NGC 507	-2	0.02	0.00	0.302	2.563	
NGC 533	-5	0.10	0.21	0.316	2.504	0.00
NGC 584	-2	0.22	0.26	0.283	2.337	1.50
NGC 596	-5	0.06	0.19	0.249	2.179	1.30
NGC 720	-5	0.22	0.29	0.330	2.392	−0.30
NGC 1052	-3	0.17	0.16	0.316	2.313	0.00
NGC 1172	-2	0.04	0.11	0.246	2.083	
NGC 1316	-2	0.12	0.15			
NGC 1395	-5	0.11	0.12	0.313	2.412	
NGC 1399	-5	0.07	0.03	0.334	2.491	
NGC 1404	-5	0.08	0.05	0.317	2.353	
NGC 1400	-3	0.04	0.06	0.309	2.398	0.00
NGC 1407	-5	0.02	0.03	0.327	2.455	−0.30
NGC 1553	-2		0.20			
NGC 1600	-5	0.19	0.17	0.324	2.506	−1.10
NGC 2314	-5	0.11	0.09	0.327	2.463	
NGC 2300	-5	0.11	0.14	0.319	2.430	1.10
NGC 2563	-2	0.16	0.14	0.330	2.416	
NGC 2629	-2	0.15	0.07	0.308	2.380	
NGC 2694	-5		0.01			
NGC 2693	-5	0.18	0.16	0.328	2.445	1.00
NGC 2832	-5	0.14	0.10	0.340	2.557	−0.40
NGC 2974	-5	0.16	0.23	0.300	2.346	0.50
NGC 3078	-5	0.19	0.08	0.334	2.376	
NGC 3115	-2	0.41	0.47	0.309	2.425	
NGC 3258	-5	0.04	0.07	0.342	2.435	0.00
NGC 3377	-5	0.27	0.24	0.270	2.116	1.55
NGC 3379	-5	0.07	0.05	0.308	2.303	0.25
NGC 3585	-3	0.24	0.26	0.308	2.343	
NGC 3607	-2	0.09	0.30	0.303	2.394	
NGC 3608	-5	0.13	0.09	0.312	2.310	−0.20
NGC 3818	-5	0.20	0.22	0.315	2.314	2.30
NGC 3894	-5	0.27	0.21	0.322	2.422	−0.70
NGC 3923	-3	0.23	0.18	0.306	2.335	−0.40
NGC 4105	-2	0.10	0.13	0.299	2.384	
NGC 4168	-5	0.04	0.08	0.260	2.259	0.80
NGC 4251	-2		0.39			2.80
NGC 4261	-5	0.09	0.05	0.330	2.468	−1.60
NGC 4291	-5	0.13	0.08	0.308	2.413	−0.40
NGC 4365	-5	0.14	0.14	0.321	2.394	−1.10
NGC 4374	-5	0.08	0.06	0.305	2.458	−0.50
NGC 4382	-2		0.11			0.80
NGC 4387	-5	0.24	0.21	0.240	1.922	−1.00
NGC 4406	-3	0.13	0.19	0.311	2.398	−0.85
NGC 4458	-5	0.10	0.04	0.227	2.027	
NGC 4467	-5	0.12	0.10	0.262	1.917	
NGC 4472	-3	0.12	0.09	0.306	2.458	−0.35
NGC 4473	-5	0.29	0.25	0.304	2.250	0.90
NGC 4550	-3		0.55			1.67
NGC 4551	-5	0.15	0.10	0.264	1.999	−0.90
NGC 4552	-2	0.02	0.04	0.324	2.417	
NGC 4564	-5	0.40	0.38	0.321	2.185	2.20
NGC 4589	-5	0.09	0.09	0.320	2.332	
NGC 4621	-5	0.19	0.16	0.328	2.381	1.50
NGC 4636	-3	0.09	0.11	0.311	2.281	−0.15
NGC 4649	-2	0.10	0.09	0.338	2.533	−0.50
NGC 4645	-5	0.24	0.21	0.273	2.233	
NGC 4697	-5	0.23	0.19	0.297	2.218	2.00
NGC 4782	-5	0.08	0.02	0.333	2.522	
IC 3896	-5	0.04	0.12		2.346	
NGC 5044	-5	0.00	0.00	0.324	2.370	
NGC 5077	-5	0.17	0.11	0.295	2.439	−0.90
NGC 5102	-2	0.24	0.49	0.005		
IC 4296	-5	0.06	0.02	0.323	2.509	
IC 4329	-2	0.15	0.24	0.336	2.447	0.80
NGC 5322	-5	0.17	0.18	0.276	2.350	−0.90
NGC 5485	-2	0.04	0.08	0.291	2.190	
NGC 5532	-2		0.00			−0.70
NGC 5576	-5	0.14	0.20	0.253	2.272	−0.50
NGC 5846	-2	0.04	0.03	0.321	2.444	
NGC 5982	-5	0.14	0.12	0.296	2.425	−0.80
NGC 6146	-2	0.16	0.10	0.289	2.435	
NGC 6876	-5	0.11	0.11	0.284	2.364	0.60
NGC 7236	-3	0.13	0.00	0.309	2.226	
NGC 7237	-3	0.03	0.00	0.327	2.234	
NGC 7332	-2		0.56			
IC 1459	-5	0.15	0.14	0.321	2.488	
NGC 7562	-5	0.18	0.18	0.291	2.385	
NGC 7619	-5	0.12	0.04	0.336	2.528	0.30
NGC 7626	-5	0.06	0.05	0.336	2.369	0.40

not also present for the full sample. A number of correlations that are present for the full sample disappeared for some of the subsamples. However, this was typically due to the decrease in the number of objects in the sample, rather than a decrease in the correlation statistic. We conclude that the strong correlations and clear noncorrelations we find are robust. It is, however, quite possible that our more marginal results would be reversed if tested with a larger sample. We urge the reader to keep this caveat in mind.

3. COMPARISONS WITH AXIAL RATIOS

3.1. *X-Ray and Optical Trends*

In Figure 1*a* we show a scatter plot of L_B against a/b. There is some evidence for a relationship in that the most luminous objects are also the roundest. Table 2 shows the results of the bivariate correlation tests on this sample: there does appear to be a statistically significant effect. If we break the sample into E and S0 subsets, we find similar distributions for both types, with the distinction that the range in axial ratio for the S0's is inevitably larger than that of the ellipticals. However, the statistical analysis of the two subsets shows no compelling evidence for correlation between L_B and a/b (see Table 2). The correlation for the full sample is only at the $\sim 1\%$ level: halving the sample size by testing the Es and S0's independently may simply reduce the sample size to the point that the correlation vanishes. Also, any intrinsic relationship between axial ratio and luminosity will be partially masked by the projection of the three-dimensional galaxies onto two dimensions. We note, however, that the most optically luminous galaxies in both subsamples are also the roundest.

The comparison of L_X with a/b is shown in Figure 1*b*. The trend with a/b noted above for L_B appears much more pronounced for L_X. Indeed, the results of the bivariate analysis (Table 2) show the effect to be much stronger than for L_B. We note that the correlation we see is not a strict linear one. It is more of a wedge: Galaxies with small a/b span the full range of L_X. Galaxies with large a/b all have $L_X \lesssim 10^{41}$ ergs s^{-1}. One might expect that this effect would be a strong function of morphology, but separation by type shows that, as well as it can be defined (given the inevitably small number of ellipticals with large a/b), the trend holds up for both ellipticals and S0's. The statistical correlation does not, however, (Table 2). It breaks down particularly for the ellipticals. We note that the only two objects with log $(a/b) \gtrsim 0.3$ (i.e., roughly E5) have fairly low X-ray upper limits. These could, however, be misclassified S0's. The trend for the S0's is weaker than for the full sample but is still significant in two of the three tests. The relationship defined by L_X/L_B is stronger than that defined by L_X (see Table 2 and Fig. 1*c*), and once again, the trend holds for both morphological subsets. More importantly, with the exception of the Cox-Hazard test for the Es, the statistical correlation holds for both subsets: For either Es or S0's alone, there is a positive correlation such that those systems with the largest L_X/L_B are the roundest objects. It is very hard to imagine how projection effects could create such a correlation, although they could easily destroy it, as apparently round galaxies could be *intrinsically* flattened, but viewed face on.

A partial-rank analysis on L_B-L_X-L_X/L_B-a/b for the full sample confirms that the underlying trend is that between L_X/L_B and a/b, in the sense that the roundest galaxies have the largest L_X/L_B (see Table A1a; see Appendix for details on this table). The bivariate trends of a/b with both L_B and L_X appear to be driven by this underlying relationship. We obtain the same results if we remove the Local Group dwarfs from the

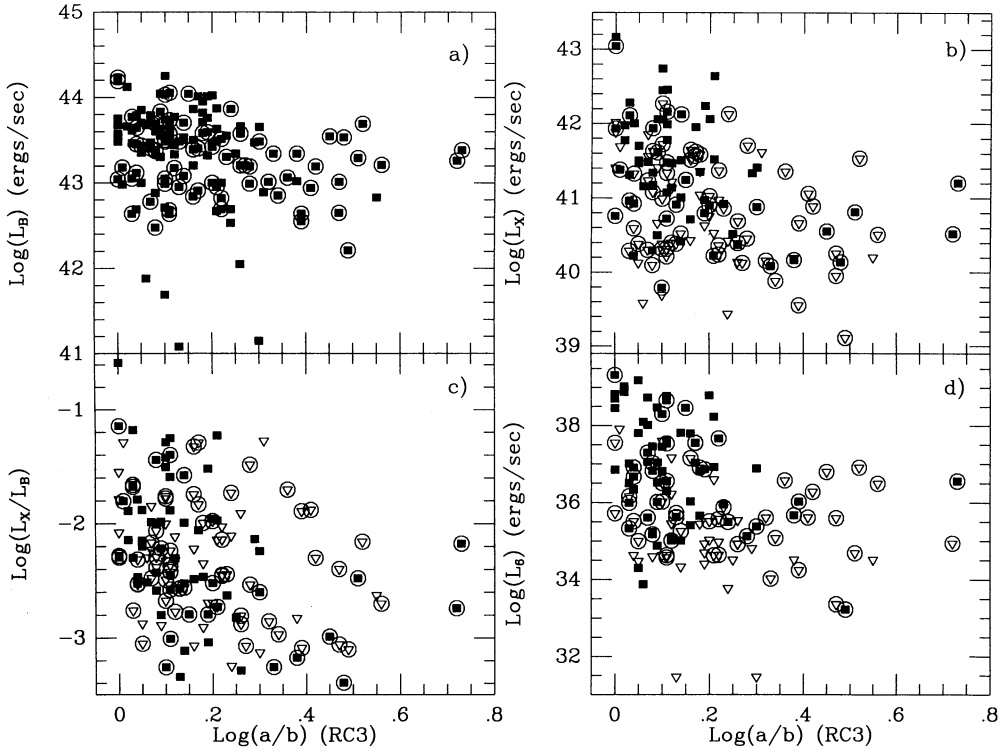

FIG. 1.—Plot of log (a/b) against (*a*) L_B, (*b*) L_X, (*c*) L_X/L_B, and (*d*) L_6 for the full sample. Solid squares represent detections. Down-pointing open triangles represent upper limits. Circled points represent the S0's.

TABLE 2

BIVARIATE CORRELATION TESTS WITH THE LUMINOSITY DATA

	L_X		L_B		L_X/L_B		L_{12}		L_{100}		L_6	
	N_{tot}	N_{lim}[b]	N_{tot}	N_{lim}	N_{tot}	N_{lim}	N_{tot}	N_{lim}	N_{tot}	N_{lim}	N_{tot}	N_{lim}
	Cox-Hazard[a]	prob		prob		prob		prob		prob		prob
	Kendall's τ	prob		prob		prob		prob		prob		prob
	Spearman rank	prob		prob		prob		prob		prob		prob
a/b	147	77	147	0	147	77	134	75	135	48	133	63
	9.727	0.0018	6.671	0.0098	14.343	0.0002	0.549	0.4587	1.724	0.1892	2.876	0.0899
	4.337	$< 10^{-4}$	3.260	0.0011	4.735	$< 10^{-4}$	1.013	0.3112	0.594	0.5522	4.960	$< 10^{-4}$
	−0.346	$< 10^{-4}$	−0.270	0.0011	−0.389	$< 10^{-4}$	−0.080	0.3544	−0.077	0.3756	−0.435	$< 10^{-4}$
Mg_2	73	26	73	0	73	26	69	39	69	28	72	26
	17.442	$< 10^{-4}$	20.965	$< 10^{-4}$	13.450	0.0002	8.786	0.0030	4.549	0.0329	12.823	0.0003
	4.395	$< 10^{-4}$	3.212	0.0013	3.962	0.0001	2.991	0.0028	1.366	0.1720	3.472	0.0005
	0.514	$< 10^{-4}$	0.361	0.0022	0.479	$< 10^{-4}$	0.372	0.0022	0.185	0.1261	0.426	0.0003
σ_v	74	27	74	0	74	27	68	39	68	29	72	27
	29.165	$< 10^{-4}$	50.449	< 10−4	21.787	$< 10^{-4}$	8.909	0.0028	11.516	0.0007	16.694	$< 10^{-4}$
	6.091	$< 10^{-4}$	5.984	< 10−4	5.072	$< 10^{-4}$	2.523	0.0116	3.166	0.0015	4.259	$< 10^{-4}$
	0.670	$< 10^{-4}$	0.634	< 10−4	0.586	$< 10^{-4}$	0.312	0.0105	0.398	0.0011	0.494	$< 10^{-4}$
a_4	47	16	47	0	47	16	46	26	46	18	47	20
	9.648	0.0019	6.287	0.0122	10.010	0.0016	2.813	0.0935	4.331	0.0374	7.338	0.0068
	2.684	0.0073	2.351	0.0187	2.397	0.0165	1.371	0.1704	1.679	0.0932	2.889	0.0039
	−0.424	0.0040	−0.324	0.0280	−0.374	0.0111	−0.218	0.1438	−0.300	0.0439	−0.381	0.0097
a_4	44	13	44	0	44	13	43	23	43	16	44	18
no dEs	15.540	0.0001	12.601	0.0004	11.426	0.0007	6.704	0.0096	5.602	0.0179	10.758	0.0010
	3.333	0.0009	3.261	0.0011	2.795	0.0052	1.878	0.0603	2.076	0.0379	3.526	0.0004
	−0.537	0.0004	−0.473	0.0019	−0.439	0.0040	−0.307	0.0466	−0.378	0.0144	−0.498	0.0011
a/b	73	31	73	0	73	31	64	36	64	24	70	29
Es only	1.017	0.3132	3.749	0.0528	0.877	0.3490	3.475	0.0623	1.572	0.2099	1.147	0.2842
	2.620	0.0088	1.411	0.1582	2.835	0.0046	1.392	0.1640	0.627	0.5307	4.117	$< 10^{-4}$
	−0.295	0.0119	−0.169	0.1484	−0.323	0.0058	−0.181	0.1500	−0.106	0.4011	−0.479	0.0001
a/b	74	47	74	0	74	47	70	39	71	24	62	34
S0s only	2.708	0.0998	2.699	0.1004	3.953	0.0468	0.066	0.7970	1.184	0.2764	6.513	0.0107
	2.978	0.0029	1.845	0.0650	3.259	0.0011	0.236	0.8134	0.474	0.6354	2.481	0.0131
	−0.329	0.0049	−0.215	0.0665	−0.343	0.0034	0.004	0.9729	−0.092	0.4400	−0.328	0.0104

[a] The values in rows (2)–(4) of these columns are the test scores for the three correlation tests.

[b] The N_{lim} are the number of limit points.

sample. Recalling that projection effects will *clearly* weaken a trend between L_X/L_B and a/b, *we find compelling evidence for a physical correlation between the presence of X-ray gas and the shape of the gravitational potential in early-type galaxies.* The trends of a/b with both L_X and L_X/L_B are significantly weakened with a_4 held constant (see Table A1a). This may be an effect of the reduction in sample size (less than a third of our full sample has a_4 measurements), or it may be due to underlying trends of both the X-ray properties and a/b with a_4. This matter is discussed further in §§ 6.1 and 6.3. An L_B-a/b trend *does* appear when pairs or triplets including the X-ray properties and either or both of Mg_2 and σ_v are held constant (see Table A1a). This trend is in the sense that more optically luminous galaxies are *flatter* for constant Mg_2 or σ_v. This is in keeping with the observation that systems with more predominant disk components (i.e., spirals) tend to have lower abundances than do ellipticals for a given luminosity.

Considering the Es only, the partial-rank analysis gives trends that are substantially weaker (see Table A1b). However, we still find evidence for trends between a/b and both L_X and L_X/L_B, with the L_X/L_B-a/b relation being the stronger. Removal of the Local Group dwarfs does not change these results. For the S0's, the trends are significantly stronger than for the Es (although weaker than for the full sample), with the L_X/L_B-a/b trend again being the dominant one (see Table A1b). This is particularly interesting, as the presence of significant disks in the S0's should make the L_X/L_B-a/b correlation more susceptible to projection than the Es. This therefore supports the conclusion that there is an underlying physical effect operating to enhance L_X/L_B is those galaxies with the roundest potentials.

3.2. *Trends with Other ISM Tracers*

The same sort of trend appears to exist between L_6 and a/b (see Fig. 1*d*), although the Cox-Hazard test is discrepant for the full sample and the Es (see Table 2). Partial-rank analysis confirms that there is a good correlation between radio power and axial ratio, independent of trends between these parameters and optical or X-ray properties (see Table A1a). This trend is in keeping with the result of Disney, Sparks, & Wall (1984) that radio-loud ellipticals tend to be significantly rounder than radio-silent ellipticals. Smith & Heckman (1989) do not confirm this result. However, they concentrate specifically on the most powerful radio galaxies, whereas both the Disney et al. sample and our own examine galaxies over a much larger range of radio power.

Knapp, Gunn, & Wynn-Williams (1992) argue quite convincingly that the bulk of the midinfrared emission from early-type galaxies is due to stellar and circumstellar radiation and thus should scale with optical luminosity (see, however the recent work of Sauvage & Thuan 1994). In P1, we found a difference at the 2 σ level between the slopes of the relationships of L_B and L_{12} with L_X that appears to be driven entirely by the S0's. Having derived a reasonably strong correlation between L_B and a/b, we have thus tested for a correlation between L_{12} and a/b. We find no evidence for such a correlation for our full sample (see Table 2). We also find no compelling evidence for correlation for either the Es or S0's tested separately, but the S0's form an essentially random sample, while the Es show at least *some* weak trend (see Table 2). If there is an underlying (if weak) relationship between the stellar luminosity (L_*) and *intrinsic* axial ratio of ellipticals/bulges, this relationship will appear weaker due to projection effects. Such a trend is suggested by the result of Kim (1988) that the *IRAS* 12 μm detection rate is significantly higher for round ellipticals than for flattened ones. For S0's, in addition to the bulge there is some contribution from the disk. If S0 disks do, in fact, have significant amounts of cool ISM (as argued in P1), then the total emission at 12 μm will be a composite of both stellar emission and diffuse emission from warm grains. The presence of a disk will make the system intrinsically flatter. Furthermore, the more prominent the disk, the more its diffuse ISM will contribute to L_{12}, and the larger its intrinsic a/b. This will work in the sense of destroying any correlation between L_{12} and a/b seen for "pure" bulge populations as a manifestation of an intrinsic L_*-a/b correlation.

We have tested our sample for a possible correlation of L_{100} with a/b and have found no evidence for any such correlation (see Table 2).

4. COMPARISONS WITH Mg_2

Mg_2 values are given for 73 of the galaxies in our sample by 7S. Figure 2*a* shows these data plotted against L_B. The point for NGC 5102 is far off-scale at (0.005, 42.2). However, as this system has an A-type spectrum (Bica & Alloin 1987), it is unlikely that the Mg_2 index measures the same physical variable as it is argued to do in typical early-type galaxies. Faber (1973) pointed out that there is a positive correlation between Mg absorption-line strength and L_B in early-type galaxies (although her original Mg_0 differs slightly from Mg_2—see Faber, Burstein, & Dressler 1977). Mg_2 is taken to be a variable of metallicity for systems in which the dominant stellar population is old (Terlevich et al. 1981; Buzzoni, Gariboldi, & Mantegazza 1992; Worthey 1994). The conversion between Mg_2 and [Fe/H] used by Terlevich et al. is taken directly from theoretical (Mould 1978) and observational (Burstein 1979) work on K giants and applied without comment to composite galaxy spectra. That of Buzzoni et al. is computed using both observations of Galactic stars, and population synthesis models covering a range of abundances and IMFs. Worthey's (1994) models indicate that the slope and zero point of such a relationship are both functions of the age of the stellar population even without variations in the IMF. Figure 3 shows the loci of the Terlevich et al. and Buzzoni et al. (with a Salpeter IMF) calibrations, and points for Worthey's (1994) models for ages from 1.5 Gyr to 17 Gyr. The agreement between the Terlevich et al. and Buzzoni et al. calibrations becomes quite poor at the lowest metallicities. However, we have only one object with $Mg_2 < 0.22$, so that is not a severe problem in our case. The Buzzoni et al. models are computed for a range of IMFs. Changing the IMF mainly affects the zero point of their Mg_2-[Fe/H] relation, such that a better agreement over our plotted range in Mg_2 is shown by assuming a shallower IMF. Also, the Worthey (1994) models for ages from 8 to 17 Gyr mainly fall between the Terlevich et al. and Buzzoni et al. calibrations.

The Mg_2 index depends on stellar surface gravity and temperature as well as both luminosity and abundance (e.g., Faber et al. 1985). Faber et al. (1985) also point out that high-resolution spectral studies often conclude that the metallicities of strong-lined stars are significantly lower than do medium- and low-resolution studies. Also, recent work (Efstathiou & Gorgas 1985; Worthey, Faber, & Gonzalez 1992; Carollo, Danziger, & Buson 1993) indicates that [Mg/Fe] is not constant among samples of elliptical galaxies. Theoretical work (Stiavelli & Matteucci 1991), and observations of the Galactic bulge (Matteucci & Brocato 1990) and of line-strength gra-

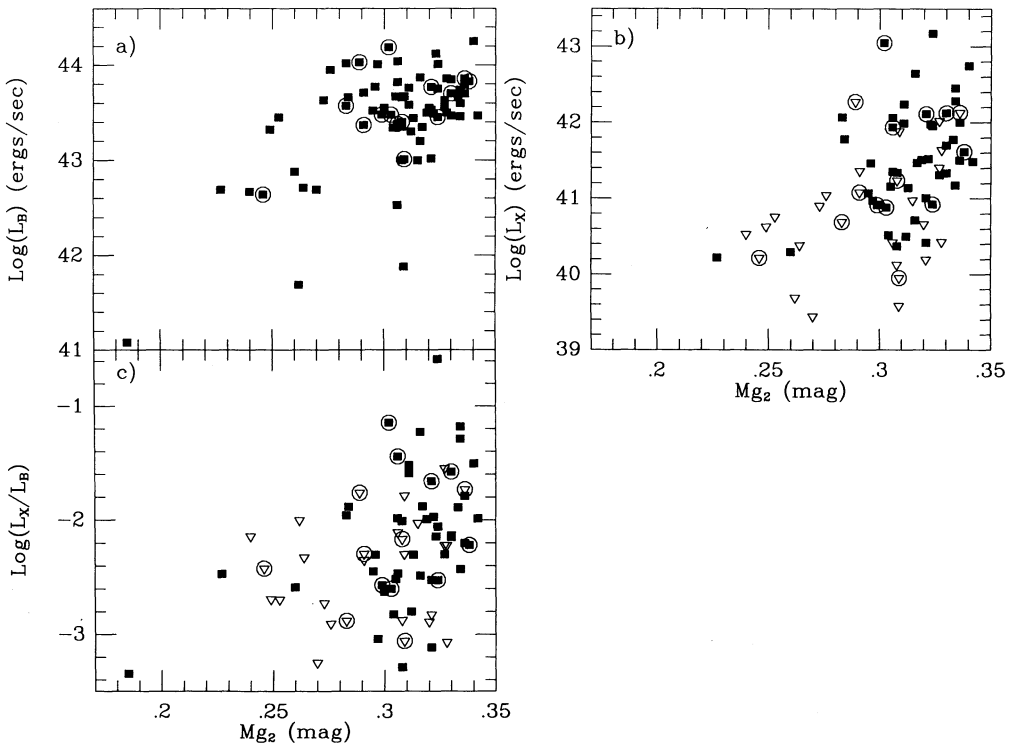

FIG. 2.—Mg_2 vs. (*a*) L_B, (*b*) L_X, and (*c*) L_X/L_B for our sample. Symbols as in Fig. 1.

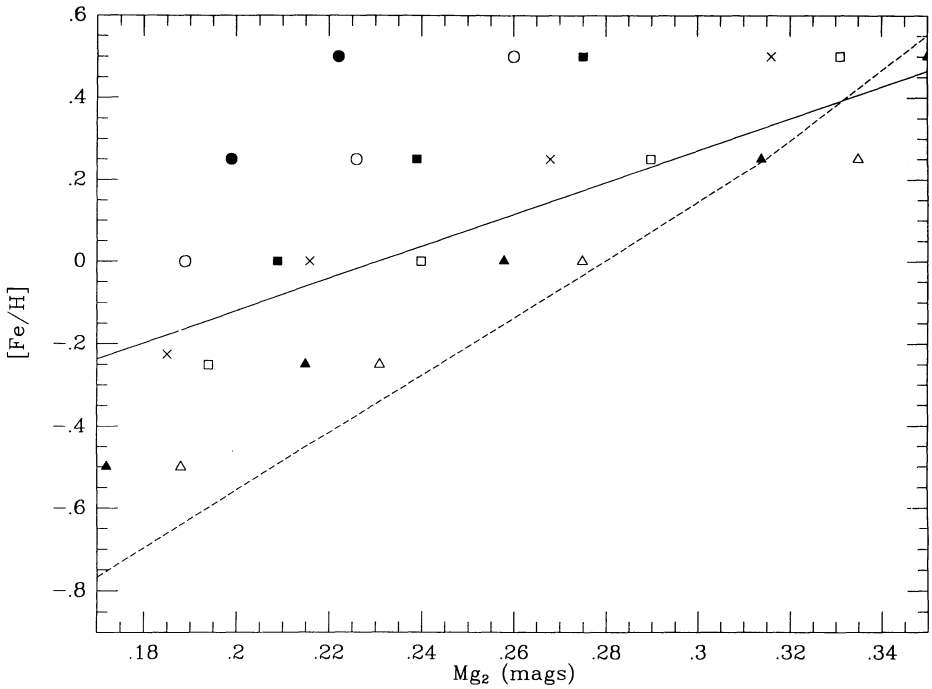

FIG. 3.—Mg_2-[Fe/H] calibrations from Terlevich et al. (1981), shown as a solid line, and Buzzoni et al. (1992) for a Salpeter IMF, shown as a dashed line. Also shown are points from the models of Worthey (1994) for a Salpeter IMF and ages of 1.5 Gyr (*solid circles*), 2 Gyr (*open circles*), 3 Gyr (*solid squares*), 5 Gyr (*crosses*), 8 Gyr (*open squares*), 12 Gyr (*solid triangles*), and 17 Gyr (*open triangles*).

dients in ellipticals (Davies, Sadler, & Petetier 1993; Carollo et al. 1993) point to Mg and Fe having very different evolutionary enrichment paths. The principal source for Mg appears to be Type II SNs (Woosley & Weaver 1986), while Type Ia and Ib SNs appear to be the source for the majority of the Fe (Nomoto, Thielemann, & Yokoi 1984; Iben et al. 1987). Furthermore, Worthey et al. (1992) and Worthey (1993) both note that their models (based on fits to field and cluster GK stars, and fits to theoretical isochrones) predict variations in [Mg/Fe] as a function of the age of a stellar population, such that older metal-rich populations will have higher [Mg/Fe] than younger ones of similar [Fe/H] (see Fig. 3). This suggests that some of the scatter in the Mg-Fe trend is due to scatter in the mixture of ages in the stellar populations of early-type galaxies. Finally, Schweizer et al. (1990) note that the magnitude and direction of the scatter about their Mg_2-M_B relationship have a negative correlation with the Σ-parameters (defined by Schweizer et al. 1990 to quantify fine structure in early-type galaxies), and Bender & Surma (1992) find evidence in four galaxies that Mg_2 increases discontinously at the same radii as the onset of kinematically decoupled cores in these galaxies. Both of these findings argue that the dynamical history of an early-type galaxy will have a significant effect on its Mg_2 strength.

As the Buzzoni et al. and Worthey (1994) models include at least some of these considerations, it is hoped that they would give a systematically more robust calibration than that of Terlevich et al. However, over the range in Mg_2 populated by our sample, the calibrations for old stellar populations differs by no more than $\lesssim$0.15 dex in [Fe/H], or less than a factor of 2. It appears from this that the use of the Mg_2 index as indicative of trends in abundance in elliptical galaxies is quite reasonable, although the results discussed above indicate that an accurate conversion of Mg_2 measurements to values of [Fe/H] is likely to be unobtainable.

4.1. *X-Ray and Optical Trends*

Accepting the above cautionary note, we conclude that our data show a correlation of higher luminosity with higher metallicity. The results of the correlation tests between Mg_2 and L_X, L_B, and L_X/L_B are given in Table 2 (NGC 5102 excluded). They all support the impression from the plots in Figure 2. The brightest systems, as well as those systems with the highest L_X/L_B, are the most metal-rich. This is generally in keeping with current notions of galaxy formation and evolution (e.g., Ferrini & Poggianti 1993 and references therein). We note that the statistically strongest correlation is that between Mg_2 and L_X. This is borne out by a partial-rank analysis on L_B-L_X-L_X/L_B-Mg_2 (see Table A2; see Appendix for details on this table). The analysis of this parameter space shows no evidence for any underlying relationship between L_B and Mg_2! The bivariate trend shown in Table 2 is entirely driven by the mutual correlations of both Mg_2 and L_B on L_X. This is a *very* curious result. It may be due to the strong nonlinear relationship between L_B and L_X ($L_X \propto L_B^{\sim 2}$—see P1). The rapid increase in X-ray flux among the most luminous galaxies could be driving the statistical outcome. Even so, this result indicates that the retention of metals produced in the initial burst of star formation and of a gravitationally bound hot ISM are physically coupled to one another. Both the existence of an X-ray halo and the retention of metals may be tied to the depth and shape of the gravitational potential. In keeping with this interpretation, we note that an L_B-Mg_2 trend *does* appear for constant a/b (see Table A2), and that the L_X-Mg_2 and L_X/L_B-Mg_2 trends tend to break down when tested for constant σ_v or a_4 (see Table A2). This matter is discussed further in §§ 5.3 and 6.3 below.

In P1 we demonstrated a correlation between L_X and the X-ray spectral shape parameter C_{21}. This parameter is defined as the ratio of counts in the 0.8–1.36 keV band to that in the 0.16–0.8 keV band (Kim et al. 1992a). The trend is in the sense that more luminous galaxies tend to have more pronounced low-energy cutoffs in their X-ray spectra. As discussed in P1, recent *ROSAT* results (e.g., Fabbiano et al. 1994; Trinchieri et al. 1994; Fabbiano & Schweizer 1994; Kim & Fabbiano 1995) suggest that this is due to a change in the intrinsic source spectrum as a function of L_X rather than to an increase in intrinsic absorption in high L_X galaxies. Another possible explanation is that galaxies with higher L_X tend also to have higher gas-phase abundances. In fact, Trinchieri, Fabbiano, & Canizares (1986) find that some of the brightest X-ray ellipticals would require gas Fe abundances substantially larger than the stellar abundances derived from Mg_2 measurements in order to reduce the derived N_H to the Galactic foreground value. It is quite possible that the two abundance scales are systematically offset. However, recent papers generally claim significantly lower abundances in the hot ISM than those determined for the stellar populations: Recent *Ginga* measurements of the 6.5 keV Fe line from NGC 1399 and NGC 4472 suggest Fe abundances between solar and 0.3 solar (Awaki et al. 1991; Ikebe et al. 1992). Results from *ROSAT* (Forman et al. 1993) are in agreement. Results for these same galaxies from BBXRT also suggest subsolar gas abundances (Serlemitsos et al. 1993). These results have, however, been questioned by Renzini et al. (1993). To explore this point further, we tested for a correlation between Mg_2 and C_{21}. The results are shown in Table 3: There is no significant bivariate correlation between these two quantities for our sample. This result is reinforced by a partial-rank analysis on L_B-L_X-L_X/L_B-Mg_2-C_{21}: again, we find no evidence for any correlation between Mg_2 and C_{21} (see Table A2). *This suggests that stronger low-energy cutoffs in X-ray–luminous early-type galaxies cannot be related solely to higher metal abundances in the X-ray–emitting gas, unless the metallicity of the ISM is totally unrelated to that of the stars.* This result has clear implications for our understanding of the X-ray spectra of early-type galaxies. In particular, it supports modelling of *ROSAT* data of X-ray–faint galaxies with multicomponent spectra, rather than with very low abundance, single-temperature models (Fabbiano et al. 1994).

4.2. *Trends with Other ISM Parameters*

The same general trend of higher luminosity with higher metallicity is also seen in all other plots of luminosity against Mg_2 (see Fig. 4). Our bivariate analysis (see Table 2) shows that, of these, the strongest relationship is between Mg_2 and L_6. This correlation is, however, weaker than that with L_X. There is some evidence that Mg_2 is correlated with L_{12}, but no significant evidence for a correlation with L_{100}. This supports the notion that the 12 μm luminosity is related to the stellar emission (e.g., Jura et al. 1987; Knapp et al. 1992). The 100 μm emission may be due to some component that is not intrinsic to the host galaxy (e.g., Forbes 1991). Alternatively, the grains radiating at 100 μm may be evaporated by the hot ISM and harsh ISRF characteristic of early-type galaxies (e.g., Boulanger et al. 1988; Knapp et al. 1992). Given that essentially all the objects with Mg_2 values from 7S in our sample are ellipticals, this is in keeping with the lack of correlation between L_X and L_{100} found in P1.

TABLE 3

BIVARIATE CORRELATION TESTS ON THE C_{21} SAMPLE

Sample	a/b N_{tot} Cox-Hazard Kendall's τ Spearman rank	N_{lim} prob prob prob	Mg_2 N_{tot}	N_{lim} prob prob prob	σ_v N_{tot}	N_{lim} prob prob prob	a_4 N_{tot}	N_{lim} prob prob prob
E+S0	39	0	28	0	28	0	19	0
	2.103	0.1470	0.646	0.4217	2.494	0.1143	1.624	0.2026
	0.984	0.3253	0.158	0.8742	1.225	0.2204	1.053	0.2922
	−0.178	0.2734	−0.030	0.8744	0.200	0.2991	−0.259	0.2710
E	24	0	22	0	22	0	17	0
	1.758	0.1849	0.122	0.7271	0.008	0.9294	0.263	0.6083
	0.722	0.4705	0.537	0.5915	0.677	0.4984	0.414	0.6792
	−0.197	0.3448	0.073	0.7382	0.106	0.6265	−0.102	0.6832
S0	15	0	6	0	6	0	2	0
	1.069	0.3011	1.305	0.2533	3.110	0.0778		
	0.698	0.4854	1.315	0.1885	1.691	0.0909		
	−0.178	0.5060	−0.429	0.3379	0.657	0.1417		

NOTE.—Table entries as defined in notes to Table 2.

4.3. *The Trend with a/b*

We see no relationship in the scatter plot of Mg_2 against a/b, and both the bivariate correlation tests (see Table 4) and partial-rank analysis (see Table A2) confirm this.

5. COMPARISONS WITH σ_v

5.1. *X-Ray and Optical Trends*

There are central velocity dispersion measurements [log (σ_v)] from 7S for 74 galaxies in our sample. Under the reasonable assumption that σ_v measures the depth of the gravitational potential well of a galaxy, and the perhaps somewhat less reasonable assumption that L_B traces the mass of the galaxy, we would expect a strong positive correlation between L_B and σ_v in our sample. This is, in fact what we find (see Fig. 5*a* and Table 2). The plots against L_X and L_X/L_B (Figs. 5*b* and 5*c*) show the same sort of relationship. The bivariate correlation analyses given in Table 2 confirm that the relationship is quite strong for L_X and L_X/L_B. Given that the sense of the correlation is maintained when we scale the X-ray luminosities by the *B*-band luminosities in our sample, we conclude that the existence of a deep potential well appears to be crucial for large L_X/L_B in early-type galaxies (see also FGT). A partial-rank analysis on L_B-L_X-L_X/L_B-σ_v reveals the trends of σ_v with L_B and L_X to be of roughly comparable strength, and stronger than that between σ_v and L_x/L_B (see Table A3; see Appendix for details on this table). These trends indicate that total luminous mass and hot ISM content are both linked to the depth of

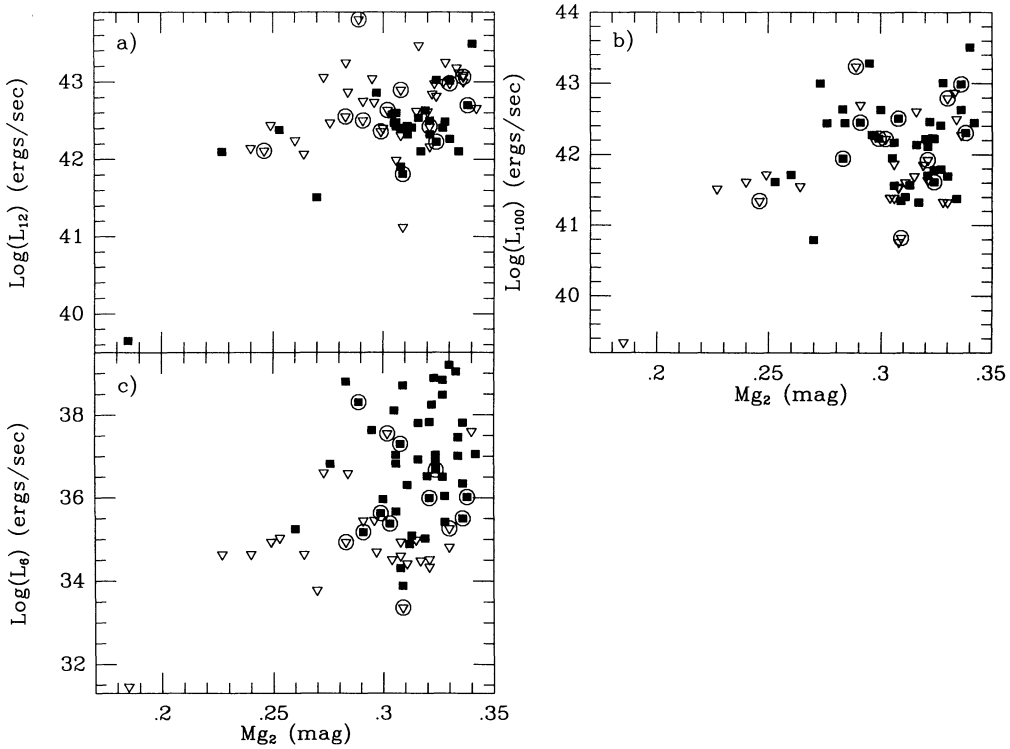

FIG. 4.—Mg_2 vs. (*a*) L_{12}, (*b*) L_{100}, and (*c*) L_6 for our sample. Symbols as in Fig. 1.

TABLE 4

BIVARIATE CORRELATION TESTS ON THE STRUCTURAL DATA

	a/b		Mg_2		σ_v	
	N_{tot}	N_{lim}	N_{tot}	N_{lim}	N_{tot}	N_{lim}
	Cox-Hazard	prob		prob		prob
	Kendall's τ	prob		prob		prob
	Spearman rank	prob		prob		prob
Mg_2	73	0				
	1.356	0.2442				
	0.940	0.3472				
	−0.101	0.3908				
σ_v	74	0	74	0		
	1.383	0.2396	46.057	$< 10^{-4}$		
	2.150	0.0316	5.284	$< 10^{-4}$		
	−0.249	0.0331	0.576	$< 10^{-4}$		
a_4	47	0	43	0	43	0
	11.247	0.0008	0.135	0.7138	8.150	0.0043
	2.510	0.0121	0.252	0.8013	2.369	0.0179
	0.374	0.0112	0.027	0.8630	−0.342	0.0265
a_4	44	0	40	0	40	0
no dEs	11.472	0.0007	0.577	0.4477	11.649	0.0006
	2.829	0.0047	0.420	0.6743	3.278	0.0010
	0.421	0.0058	−0.079	0.6201	−0.515	0.0013

NOTE.—Table entries as defined in notes to Table 2.

the potential well; a satisfying, if not terribly surprising result. The L_X-σ_v and L_X/L_B-σ_v trends do tend to weaken somewhat when tested for constant a_4, but this appears to be due mainly to the decrease in sample size (from 73 to 40 objects) when a_4 is considered.

5.2. *Trends with Other ISM Parameters*

For the 6 cm data, the distribution looks more like a threshold relation than a linear correlation (see Fig. 6). For log $(\sigma_v) \lesssim 2.2$ (measured in km s^{-1}) there are no detected 6 cm radio sources with luminosities greater than 10^{35} ergs s^{-1}. Above this threshold, there are immediately systems with 6 cm luminosities of $\approx 10^{39}$ ergs s^{-1}. The *IRAS* data at both 12 μm and 100 μm (also shown in Fig. 6) suggest positive correlations also, but do not appear as strong as those with either L_X or L_6. This impression is confimed by the bivariate analysis in Table 2: The correlations with the *IRAS* luminosities are significant at the 0.1%–1% level. The optical, radio, and X-ray corre-

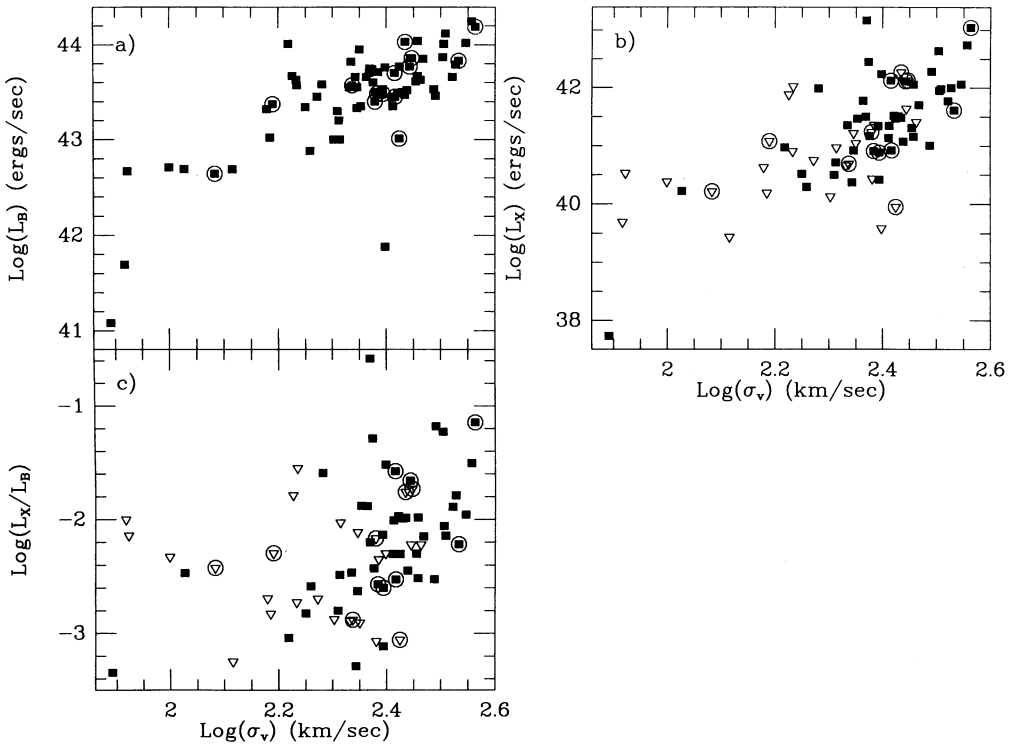

FIG. 5.—σ_v vs. (*a*) L_B, (*b*) L_X, and (*c*) L_X/L_B for our sample. Symbols as in Fig. 1.

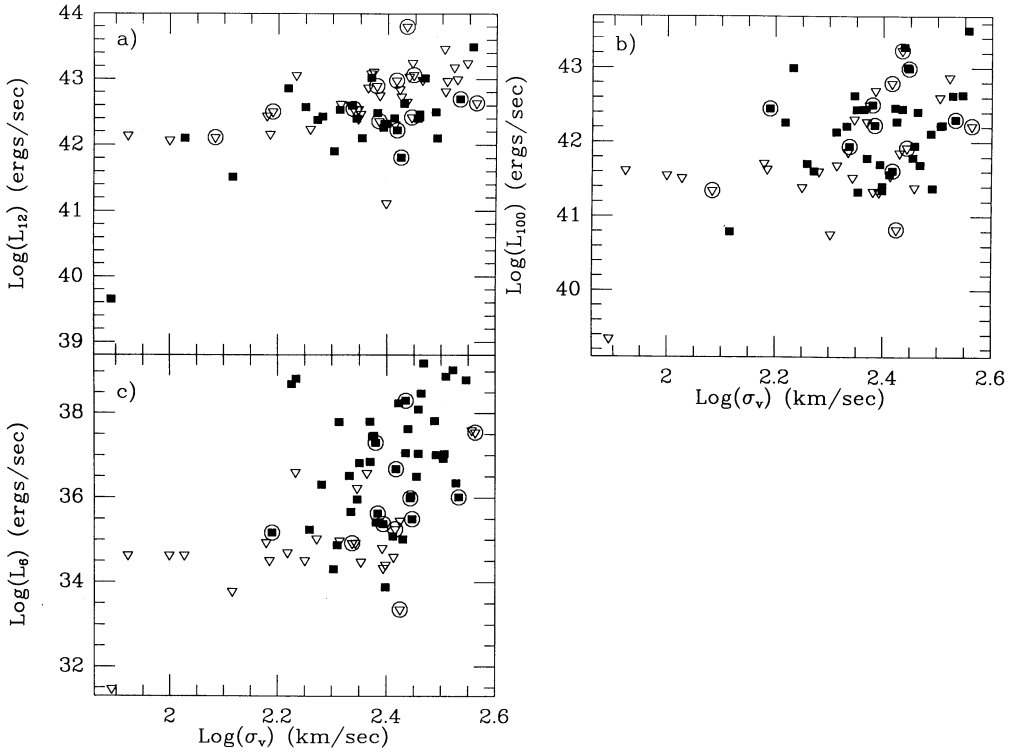

FIG. 6.—σ_v vs. (*a*) L_{12}, (*b*) L_{100}, and (*c*) L_6 for our sample. Symbols as in Fig. 1.

lations are all significant at levels of $<0.01\%$. This suggests a picture in which the fuel source (cooling X-ray gas) and feeding rate (which determines the radio power) of the central engine are both directly coupled to the central potential depth, in keeping with the notions of FGT.

5.3. *Trends with Other Structural Parameters*

It is not surprising that we should find a good correlation between Mg_2 and σ_v for our sample, given that these data are drawn from 7S, who find such a correlation for their full sample (also see Bender 1992). The results for our objects are shown in Figure 7*b* and Table 4. It is somewhat surprising that the correlation between a/b and σ_v is so weak, however (see Fig. 7*a* and Table 4). While there is a general trend for the galaxies with the largest values of σ_v to be the roundest, the data are not at all compelling. Partial-rank analysis shows that the only example of a significant a/b-σ_v trend occurs for constant L_B, in the sense that galaxies with deeper potential wells tend to be rounder than those with shallow potential wells. This could be because there is more internal support from rotation in the flatter systems at a given luminosity. There is a very strong correlaton between Mg_2 and σ_v for all tested combinations (see Table A3); see Appendix for details on this table).

6. COMPARISONS WITH a_4

6.1. *X-Ray and Optical Trends*

We have taken measurements of the amplitude of the cos (4 θ) Fourier term of the isophotal deviations from ellipticity for 47 galaxies in our sample from the papers of Bender et al. (1989) and Peletier et al. (1990). These data are given in Table 1. These a_4 values are measured from isophotes at $\lesssim 2r_e$ (typically $\sim 0.5r_e$ for the Peletier et al. sample), and thus describe the morphology of the inner parts of these galaxies. In Figure 8*a* we show that our sample is representative of the full samples of these earlier studies in that more luminous ellipticals tend to be boxy (have negative a_4 terms), while the less luminous tend to be disky (positive a_4). The exceptions to this are three boxy dwarf ellipticals, marked in the figure. Recent work (e.g., Bender & Nieto 1990; Carter & Sadler 1990; Held, Mould & de Zeeuw 1990; Bender, Paquet, & Nieto 1991) indicates that these galaxies do not fall along a simple extension of the properties of giant ellipticals. This deviation is therefore neither surprising nor (for the work discussed here!) terribly significant.

Bender et al. (1989) comment that they see a relationship between L_X and a_4 for their sample. They do not test for such a relationship, possibly due to the very small number of objects for which they had X-ray data. Our sample is substantially larger (see Figs. 8*b* and 8*c*). The results of the bivariate correlation analysis of a_4 with L_B, L_X, and L_X/L_B are given in Table 2. This analysis confirms the assertion of Bender et al. (1989) that X-ray–luminous galaxies tend to be boxier than X-ray–faint galaxies at the $\sim 0.1\%$ level if the dE's are not included. The strength of the bivariate correlation with L_B is marginally worse than that with L_X. The trend with L_X/L_B, again in the sense that the galaxies with the highest L_X/L_B tend to be boxy, is statistically the weakest of the three, but the correlation is *still* significant at a level of $\lesssim 0.5\%$ for all three tests. Partial-rank analysis on L_B-L_X-L_X/L_B-a_4 reveals that the trend of L_X with a_4 is the strongest of the three and appears to drive the other two (see Table A4; see Appendix for details on this table). The L_X-a_4 trend breaks down when tested for constant σ_v. We noted in § 5.1 that there is a strong L_X-σ_v trend. This trend is maintained for constant a_4 (see Table A3), arguing that an underlying trend between a_4 and σ_v is driving the L_X-a_4 correlation. We explore this result further in § 6.3 below.

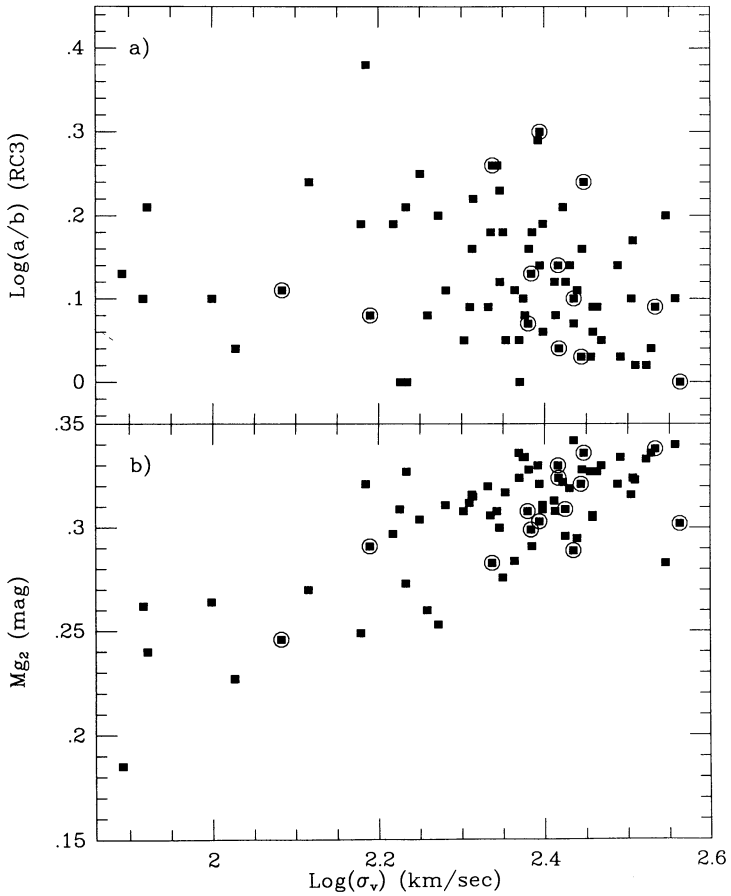

FIG. 7.—σ_v vs. (*a*) a/b, and (*b*) Mg_2 for our sample. Symbols as in Fig. 1.

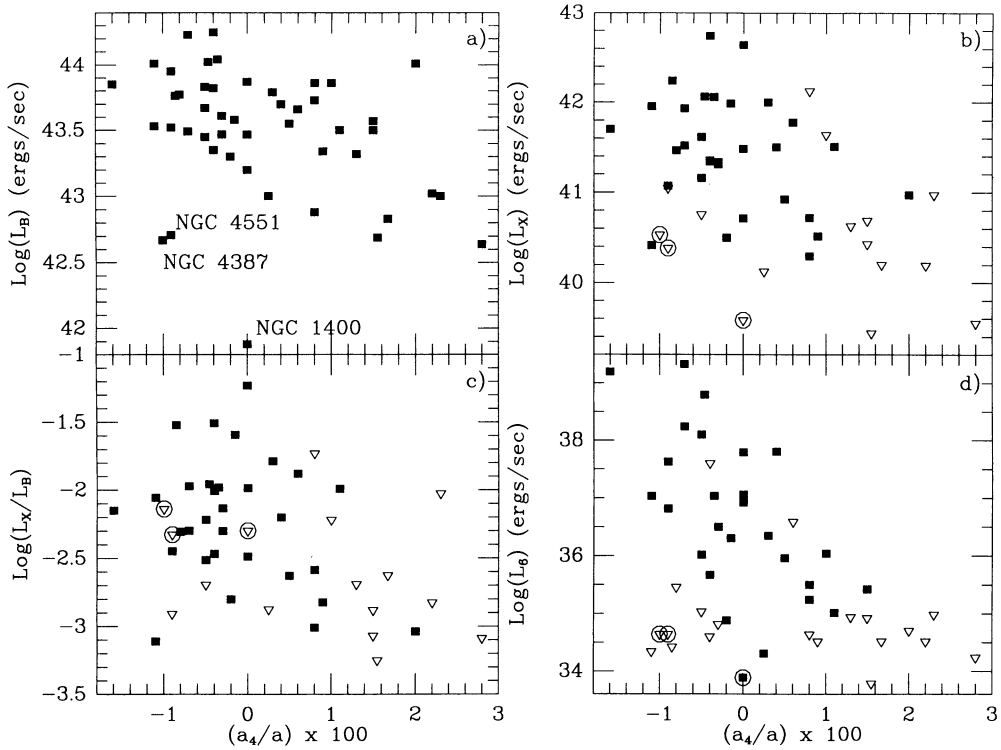

FIG. 8.—a_4 vs. (*a*) L_B, (*b*) L_X, (*c*) L_X/L_B, and (*d*) L_6 for our sample. The dwarf ellipticals are identified in (*a*), and circled in (*b*), (*c*), and (*d*). All other symbols as in Fig. 1.

6.2. *Trends with Other ISM Parameters*

There are trends of marginal statistical significance between a_4 and both L_{12} and L_{100}, at the $\lesssim 6\%$ and $\lesssim 4\%$ confidence levels respectively (see Table 2). A strong trend is apparent between a_4 and L_6 in Figure 8*d*. This correlation is confirmed at roughly the 0.1% level (Table 2). There are *no* high-luminosity 6 cm sources in our sample that are disky galaxies. This is in keeping with previous findings that central radio sources are more prevalent in ellipticals without disk features (Peletier et al. 1990). A partial-rank analysis including L_6 indicates that the relationship between L_6 and a_4 is stronger than that between L_B and a_4 (see Table A4), although weaker than the L_X-a_4 correlation: Boxy galaxies generate more radio power than disky galaxies of the same optical and X-ray luminosities.

The picture that emerges from our consideration of the relationship of structural parameters to the luminosities in our various wavebands is that L_B, L_X, L_X/L_B, and L_6 *are correlated with both the depth of the potential* (*as measured by* σ_v *and* Mg_2) *and the shape of the potential* (*as measured by* a/b *and* a_4).

6.3. *Trends with Other Parameters*

We find a correlation at the $\sim 0.5\%$ level (see Table 4) between a_4 and a/b in the sense that rounder galaxies tend to be boxy, and flatter galaxies tend to be disky. This is not a tautology: recall that a/b simply measures the ratio of the projected major and minor axes of a system; a_4 measures the extent and sense of deviation of the isophotes of a system from pure elliptical symmetry. It is entirely possible, from a mathematical point of view, for a system with high ellipticity to have boxy isophotes, or one with very low ellipticity to have disky isophotes. The data are shown in Figure 9*a*. A partial-rank analysis on L_B-L_X-L_X/L_B-a/b-a_4 supports this picture (see Tables A1 and A4) but suggests that the a/b-a_4 trend may be largely driven by underlying relationships of both a_4 and a/b with the luminosity parameters.

Much to our surprise, the data show no indication for a correlation between a_4 and Mg_2 (see Fig. 9*b* and Table 4). One might expect there to be a relationship between these such that boxy galaxies would tend to have higher Mg_2 than disky galaxies. Indeed, Sil'chenko (1994) finds some evidence for just such a result. However, if anything, the data we have show an opposite trend: the lowest values of Mg_2 tend to be from boxy galaxies. Overall, though, there is no indication from this sample for any significant trend. A partial-rank analysis on L_B-L_X-L_X/L_B-a/b-a_4-Mg_2 confirms this result (see Table A4).

With the exception of two dwarf galaxies, we see a steep correlation between a_4 and σ_v for our sample (see Fig. 9*c*), in the sense that boxy galaxies tend to have large velocity dispersions. For the full sample this correlation is significant at the $\sim 2.7\%$ level (see Table 4). Removing the dwarfs galaxies improves this to a $\sim 0.1\%$ correlation. A partial-rank analysis on L_B-L_X-L_X/L_B-a/b-a_4-σ_v suggests that this correlation may be the underlying cause of the observed relation between a_4 and a/b (see Table A4). Testing L_B-L_X-L_X/L_B-a/b-a_4-Mg_2-σ_v, we find statistical evidence for a positive correlation between a_4 and Mg_2 at the $\sim 4\%$–5% level. We note that this correlation appears *only* when we test for a constant σ_v. This therefore implies that, *for a given potential depth*, disky galaxies have *higher* metallicity *or* older stellar populations than boxy galaxies. We also note that the strongest σ_v-a_4 correlations all result when tested with constant Mg_2 (see Table A4). The effect of Mg_2 can be seen in Figure 9*c* where the points enclosed in

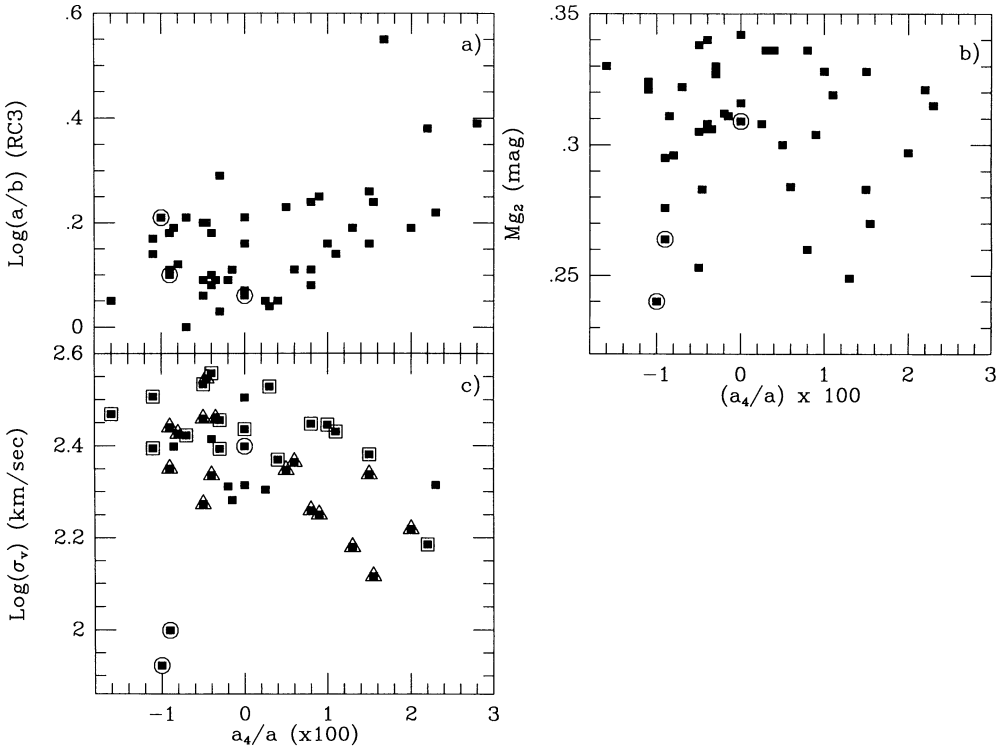

FIG. 9.—a_4 vs. (*a*) a/b, (*b*) Mg_2, and (*c*) σ_v for our sample. Symbols as in Fig. 8. In (*c*) the points enclosed in squares are the systems with the highest 40% of Mg_2 values; those enclosed in triangles are the lowest 40%.

squares are the 40% of the sample with the largest Mg_2 values, and those enclosed in triangles are the 40% with the smallest Mg_2 values. For a given a_4 value, the high-Mg_2 objects have systematically higher σ_v than the low-Mg_2 objects.

One possible interpretation of these results is suggested by the hypothesis that boxy ellipticals are the product of mergers of smaller systems, while disky ellipticals are "primordial" in the sense that the overall morphology of the system is a reflection of its state at the epoch of galaxy formation (e.g., Nieto & Bender 1989; Kormendy & Djorgovski 1989; Barnes & Hernquist 1992). At the present epoch, there appears to be a mass-abundance relationship amongst galaxies of a given morphology (e.g., Faber 1973; Wyse & Silk 1985; Dekel & Silk 1986; DeYoung & Gallagher 1990; Franx & Illingworth 1990) such that less massive systems are less metal-rich. If such a relationship has always held, then the formation of a boxy E of some mass M from two smaller objects would result in a *lower* abundance galaxy than a disky E of the same mass M if the bulk of the stars in the boxy galaxy had already formed *before* the merger. Furthermore, boxy galaxies that formed from the merging of lower mass progenitors will result in objects with lower current stellar abundances compared to those formed from the merging of higher mass progenitors, because a larger fraction of the enriched ejecta from the initial merger induced burst of star formation will escape from their shallower potential wells.

A second possibility is that disky systems are the products of mergers involving at least one disk galaxy, in which either the self-gravitating part of the disk survives the accretion event (as may be the case in Cen A), or the ISM undergoes dissipational collapse to form a new central disk system (e.g., Hernquist & Barnes 1991). This is the most reasonable explanation for galaxies with kinematically decoupled cores (e.g., Bender 1990; Bertola 1992) and may hold for disky galaxies in general. This is because both the studies of Bender et al. (1989) and Peletier et al. (1990) determine the a_4 parameter at fairly small radii. Bender et al. (1989) state that all their a_4 values are computed from isophotes within $2r_e$. Peletier et al. (1990) publish the radii at which they determined a_4. The mean is $\sim 0.5r_e$, with a few as low as $0.1r_e$, and only three of 35 galaxies $\geq 1r_e$. Thus "disky" systems are so labeled because their inner isophotes have disk features. Several of the systems with negative a_4 from the Bender et al. (1989) sample have very boxy isophotes at large radii (F. Schweizer 1994, private communication) and thus appear to be merger remnants on that criterion. Bender & Surma (1992) observed four ellipticals with kinematically decoupled cores and found a sharp increase in the Mg_2 line strengths at the same radii at which the peculiar kinematics appear. As the Mg_2 values from 7S are all nuclear values, the trend of higher Mg_2 line strengths in disky systems at a given σ_v may be due to higher abundances in the captured or secondary nuclear disks of merger remnants with disky central isophotes.

7. SUMMARY AND SUGGESTIONS FOR FUTURE RESEARCH

1. Rounder galaxies tend to have larger L_X, L_X/L_B, and L_6. Partial-rank analysis shows the L_X/L_B-a/b trend to be the strongest of the three. This suggests a connection between the shape of the potential and the ability to retain substantial halos of hot ISM. These in turn could be responsible for both feeding the nuclear sources through cooling flows and confining radio lobes (see also FGT). The same general trends hold for correlations with a_4, but the strongest trend here is that between a_4 and L_X (confirming the observation of Bender et al. 1989).

2. Axial ratio (a/b) and boxiness (a_4) are correlated in the sense that flatter galaxies tend to have diskier isophotes. Partial-rank analysis suggests that the trends between a_4 and a/b may be driven by underlying relationships of both axial ratio and a_4 with the luminosity parameters.

3. Both a/b and a_4 are correlated with L_B but are not strongly correlated with either L_{12} or L_{100}. The lack of any strong trend with L_{12}, and the results of P1, indicate that there may be some significant contribution to the 12 μm emission from hot dust in early-type galaxies that is not directly related to the stellar component. For the S0's, there may be a contribution from dust associated with disk star formation regions. The lack of trends with L_{100} is consistent with the notion that the FIR-emitting material is accreted (e.g., Forbes 1991), or that it is evaporated by the hot ISM and hard ISRF on fairly short timescales (e.g., Knapp et al. 1992).

4. There are strong correlations between Mg_2, σ_v, and L_X. Partial-rank analysis shows that the depth of the potential well is the crucial parameter. From a physical standpoint, the deeper the potential well, the better a galaxy is able to retain its hot ISM at the current epoch (the L_X-σ_v correlation), and the better it was able to retain the enriched ejecta from its initial phase of strong star formation, and reprocess this ejecta into new stars (the Mg_2-σ_v correlation).

5. There is no significant correlation between the X-ray spectral parameter C_{21} and Mg_2. C_{21} is defined by Kim et al. (1992a) as the ratio of emission in the 0.8–1.36 keV band to that in the 0.16–0.8 keV band and thus measures the shape of the X-ray spectrum in this region. The lack of correlation between C_{21} and Mg_2 suggests that the relative absence of low-energy cutoffs in X-ray–faint early-type galaxies (see Kim, Fabbiano, & Trinchieri 1992b) is not related to lower abundances in the X-ray–emitting gas, unless the metallicity of the ISM is unrelated to that of the stars. This supports the conclusion of Fabbiano et al. (1994) that X-ray–faint ellipticals have complex X-ray spectra.

6. Many of the trends we find are "wedgelike" or "threshold-like" rather than being a simple power law. One of the most impressive of these is the L_6-σ_v trend discussed in § 5.2. We find a threshold of $\log(\sigma_v) \approx 2.2$ above which the maximum radio luminosities in our sample jump abruptly by more than an order of magnitude. Below this value of σ_v, it appears that the potential well is too shallow to efficiently transport material to the nuclear engine. It does not seem coincidental that, at this same value of σ_v, we see a jump in the maximum detected L_X/L_B of more than one order of magnitude.

7. X-ray, radio, and optical luminosities are all correlated with both shape (a/b, a_4), and depth (Mg_2, σ_v) parameters. There are also strong relationships among the shape and the depth parameters. However, trends between the shape parameters (a/b, a_4) and one of the depth parameters (Mg_2 or σ_v) are modulated by the other parameter. That is, for instance, at a given a_4 value, the spread in σ_v appears directly related to the spread in Mg_2 such that the higher σ_v objects also have higher Mg_2. Alternatively, for a given σ_v, boxy galaxies tend to have *lower* Mg_2 values (and thus, we surmise, lower stellar abundances) than disky galaxies. This suggests that the presence of a hot ISM is dependent on both the shape (a/b, a_4) and the depth (Mg_2, σ_v) of the potential, but that these two families of parameters are not related in a simple way.

The nature of the coupling between the shape and depth parameters is clearly an important input for understanding the formation and evolution of early-type systems. A galaxy may have a deep potential either because of initial conditions (the result of a large primordial fluctuation) or because it is the product of mergers of a number of less massive objects. We observe that Es with disky inner isophotes have larger nuclear Mg_2 strengths than galaxies with boxy inner isophotes at a given σ_v. If disky isophotes signal "primordial" ellipticals (ones that have not experienced significant merging since the epoch of galaxy formation) and boxy isophotes signal systems that have been built up by mergers, two possible explanations of this result suggest themselves. First, if the presently observed mass-abundance relationship for galaxies is a relic of a fundamental constraint of the galaxy formation process, then a disky elliptical of a given mass could have a higher average central stellar abundance than a merger product (a boxy elliptical) of the same mass that was formed from lower mass (and thus lower abundance) precursors. Second, boxy ellipticals could have lower Mg_2 values for a given [Fe/H] due to an overall younger stellar population resulting from merger-induced star formation bursts. Alternatively, if disky isophotes signal merger systems that have either formed secondary nuclear disks (see Hernquist & Barnes 1991), or captured self-gravitating spiral disks, then the enhancement of nuclear Mg_2 strengths at a given σ_v may be due to high abundances in those disks (see Bender & Surma 1992).

Various avenues present themselves for further study of these possibilities. One that we are pursuing is the comparison of the database from this work and P1 with the dynamically motivated κ-parameters defined by Bender, Burstein, & Faber (1992). It would also be very interesting to study the radial gradients of Mg_2 and σ_v for early-type galaxies with a range in X-ray properties and to look for other signs of fine structure (as discussed by, e.g., Schweizer & Seitzer 1992) as a function of X-ray properties. Such studies ought to make great contributions to our understanding of the formation histories and physical evolution of early-type galaxies.

We would like to thank Glen Mackie and Ginevra Trinchieri for their comments on this study as it has progressed, and François Schweizer for stimulating comments and a critical reading of the manuscript. We would also like to thank Eric Feigelson and Michael LaValley for providing us with the latest versions of the ASURV software package. G. F. would like to thank the Aspen Summer School for the opportunity to focus on this project. P. B. E. would like to thank the organizers and participants of the Third Teton Summer School, where easly results of this project were discussed. This research has made use of the NASA/IPAC Extragalactic Database (NED) which is operated by the Jet Propulsion Laboratory, Caltech, under contract with the National Aeronautics and Space Administration. We are grateful to the National Aeronautics and Space Administration for suport of this research under the LTSA grant NAGW 2681 and contract NAS 8-39073 (AXAF Science Center).

TABLE A1a

PARTIAL SPEARMAN RANK ANALYSIS: TRENDS WITH log (a/b), E + S0 SAMPLE

Test Pair	Held parameters	Size	Paritial Spearman rank	Probability
L_B–a/b	L_X	147	−0.047	0.287
	L_X/L_B	147	−0.108	0.099
	Mg_2	73	0.066	0.292
	σ_v	74	0.176	0.072
	a_4	44	−0.138	0.199
	L_X,L_X/L_B	147	−0.030	0.361
	L_X,Mg_2	73	0.254	0.019
	L_X,σ_v	74	0.277	0.010
	L_X,a_4	44	0.024	> 0.400
	L_X/L_B,Mg_2	73	0.197	0.051
	L_X/L_B,σ_v	74	0.231	0.026
	L_X/L_B,a_4	44	−0.063	0.349
	L_6,a_4	44	−0.004	> 0.400
	Mg_2,σ_v	73	0.164	0.090
	Mg_2,a_4	40	0.057	0.368
	σ_v,a_4	40	0.197	0.125
	L_X,L_X/L_B,Mg_2	73	0.278	0.010
	L_X,L_X/L_B,σ_v	74	0.282	0.009
	L_X,L_X/L_B,a_4	44	0.015	> 0.400
	L_X,L_6,a_4	44	0.076	0.319
	L_X,Mg_2,σ_v	73	0.274	0.012
	L_X,Mg_2,a_4	40	0.120	0.241
	L_X,σ_v,a_4	40	0.211	0.108
	L_X/L_B,L_6,a_4	44	0.026	> 0.400
	L_X/L_B,Mg_2,σ_v	73	0.223	0.035
	L_X/L_B,Mg_2,a_4	40	0.098	0.283
	L_X/L_B,σ_v,a_4	40	0.200	0.125
	Mg_2,σ_v,a_4	40	0.170	0.169
	L_X,L_X/L_B,L_6,a_4	44	0.070	0.336
	L_X,L_X/L_B,Mg_2,σ_v	73	0.283	0.010
	L_X,L_X/L_B,Mg_2,a_4	40	0.116	0.249
	L_X,L_X/L_B,σ_v,a_4	40	0.201	0.127
	L_X,Mg_2,σ_v,a_4	40	0.182	0.155
	L_X/L_B,Mg_2,σ_v,a_4	40	0.173	0.168
	L_X,L_X/L_B,Mg_2,σ_v,a_4	40	0.173	0.171

APPENDIX

Tables A1–A4 contain the detailed results of the partial Spearman rank statistical analysis. Table A1 shows the analysis of L_B-a/b, L_X-a/b, L_X/L_B-a/b, and L_6-a/b. Table A2 shows L_B-Mg_2, L_X-Mg_2, L_X/L_B-Mg_2, C_{21}-Mg_2, and a/b-Mg_2. Table A3 shows L_B-σ_v, L_X-σ_v, L_X/L_B-σ_v, a/b-σ_v, and Mg_2-σ_v. Table A4 shows L_B-a_4, L_X-a_4, L_X/L_B-a_4, L_6-a_4, a/b-a_4, Mg_2-a_4, and σ_v-a_4. The tables are organized into sections, with each section showing correlation probabilities for a given pair of inputs (for instance, L_B-a/b in Table A1). Within each section, column (1) identifies the test pair, column (2) identifies the quantities to be held constant in the test, column (3) gives the number of objects in the sample, column (4) gives the partial Spearman rank statistic, and column (5) gives the probability that the test pair show a correlelation for that set of parameters.

Tables A1–A4 are published in their entirety in computer-readable form in the AAS CD-ROM Series, Volume 4. A portion of Table A1a appears on the preceding page.

REFERENCES

Awaki, H., Koyama, K., Kunieda, H., Takano, S., Tawara, Y., & Ohashi, T. 1991, ApJ, 336, 88
Barnes, J. E., & Hernquist, L. 1992, ARA&A, 30, 705
Bender, R. 1990, in Dynamics and Interactions of Galaxies, ed. E. R. Weilen (Heidelberg: Springer), 249
———. 1992, in IAU Symp. 149. The Steller Populations of Galaxies, ed. B. Barbuy & A. Renzini (Dordrecht: Kluwer), 267
Bender, R., Burstein, D., & Faber, S. M. 1992, ApJ, 399, 462
Bender, R., & Nieto, J.-L. 1990, A&A, 239, 97
Bender, R., Paquet, A., & Nieto, J.-L. 1991, A&A, 246, 349
Bender, R., & Surma, P. 1992, A&A, 258, 250
Bender, R., Surma, P., Döbereiner, S., Möllenhoff, C., & Madejesky, R. 1989, A&A, 217, 35
Bertola, F. 1992, in Morphology and Physical Classification of Galaxies, ed. G. Longo, M. Capaccioli, & G. Busarello (Dordrecht: Kluwer), 115
Bica, E., & Alloin, D. 1987, A&AS, 70, 281
Boulanger, F., Beichman, C., Désert, F. X., Helou, G., Pérault, M., & Ryter, C. 1988, ApJ, 332, 328
Burstein, D. 1979, ApJ, 232, 74
Buzzoni, A., Gariboldi, G., & Mantegazza, L. 1992, AJ, 103, 1814
Carollo, C. M., Danziger, I. J., & Buson, L. 1993, MNRAS, 265, 553
Carter, D., & Sadler, E. M. 1990, MNRAS, 245, 12P
Ciotti, L., D'Ercole, A., Pellegrini, S., & Renzini, A. 1991, ApJ, 376, 380
Davies, R. L., Sadler, E. M., & Peletier, R. F. 1993, MNRAS, 262, 650
Dekel, A., & Silk, J. 1986, ApJ, 303, 39
de Vaucouleurs, G., de Vaucouleurs, A., & Corwin, H. G. 1976, Second Reference Catalogue of Bright Galaxies (Austin: University of Texas Press)
de Vaucouleurs, G., de Vaucouleurs, A., Corwin, H. G., Jr., Buta, R. J., Paturel, G., & Fouqué, P. 1991, Third Reference Catalogue of Bright Galaxies (New York: Springer (RC3)
DeYoung, D., & Gallagher, J. 1990, ApJ, 356, L15
Disney, M. J., Sparks, W. B., & Wall, J. V. 1984, MNRAS, 206, 899
Eder, J. A., Giovanelli, R., & Haynes, M. P. 1991, AJ, 102, 572
Efstathiou, G., & Gorgas, J. 1985, MNRAS, 215, 37P
Eskridge, P. B., Fabbiano, G., & Kim, D.-W. 1995, ApJS, in press (P1)
Fabbiano, G. 1989, ARA&A, 27, 87
———. 1994, in New Horizons of X-Ray Astronomy: First Results from *ASCA*, ed. F. Makino & T. Ohashi (Tokyo: Universal Academy), 159
Fabbiano, G., Gioia, I. M., & Trinchieri, G. 1988, ApJ, 324, 749
———. 1989, ApJ, 347, 127 (FGT)
Fabbiano, G., Kim, D.-W., & Trinchieri, G. 1992, ApJS, 80, 531 (P0)
———. 1994, ApJ, 429, 94
Fabbiano, G., & Schweizer, F. 1995, ApJ, submitted
Faber, S. M. 1973, ApJ, 179, 731
Faber, S. M., Burstein, D., & Dressler, A. 1977, AJ, 82, 941
Faber, S. M., Friel, E. D., Burstein, D., & Gaskell, C. M. 1985, ApJS, 57, 711
Faber, S. M., Wegner, G., Burstein, D., Davies, R. L., Dressler, A., Lynden-Bell, D., & Terlevich, R. J. 1989, ApJS, 69, 763 (7S)
Feigelson, E. D., & Babu, G. J. 1992, Statistical Challenges in Modern Astronomy (New York: Springer)
Feigelson, E. D., & Nelson, P. I. 1985, ApJ, 293, 192
Ferrini, F., & Poggianti, B. M. 1993, ApJ, 410, 44
Forbes, D. A. 1991, MNRAS, 249, 779
Forman, W., Jones, C., David, L., Franx, M., Makishima, K., & Ohashi, T. 1993, ApJ, 418, L55
Franx, M., & Illingworth, G. 1990, ApJ, 359, L41
Giacconi, R., et al. 1979, ApJ, 230, 540
Goudfrooij, P., Hansen, L., Jørgensen, H. E., & Nørgaard-Nielsen, H.-U. 1994, A&AS, 105, 341
Held, E. V., Mould, J. R., & de Zeeuw, P. T. 1990, AJ, 100, 415
Hernquist, L., & Barnes, J. E. 1991, Nature, 354, 210
Huchtmeier, W. K., & Richter, O.-G. 1989, A General Catalog of H I Observations of Galaxies (New York: Springer)
Iben, I., Jr., Nomoto, K., Tornambè, A., & Tutukov, A. 1987, ApJ, 317, 717
Ikebe, Y., et al. 1992, ApJ, 384, L5
Isobe, T., Feigelson, E. D., & Nelson, P. I. 1986, ApJ, 306, 490
Jura, M., Kim, D.-W., Knapp, G. R., & Guhathkurta, P. 1987, ApJ, 312, L11
Kendall, M., & Stuart, A. 1976, The Advanced Theory of Statistics, Vol. 2 (New York: Macmillan)
Kim, D.-W. 1988, Ph.D. thesis, Univ. California, Los Angeles
Kim, D.-W., & Fabbiano, G. 1990, in Windows on Galaxies, ed. G. Fabbiano, J. S. Gallagher, & A Renzini (Dordrecht: Kluwer), 293
———. 1995, ApJ, 441, 182
Kim, D.-W., Fabbiano, G., & Trinchieri, G. 1992a, ApJS, 80, 645
———. 1992b, ApJ, 393, 134
Knapp, G. R., Guhathakurta, P., Kim, D.-W., & Jura, M. 1989, ApJS, 70, 329
Knapp, G. R., Gunn, J. E., & Wynn-Williams, C. G. 1992, ApJ, 399, 76
Kormendy, J., & Djorgovski, S. 1989, ARA&A, 27, 235
LaValley, M. P., Isobe, T., & Feigelson, E. D. 1992, BAAS, 24, 839
Matteucci, F., & Brocato, E. 1990, ApJ, 365, 539
Mould, J. R. 1978, ApJ, 220, 434
Nieto, J.-L., & Bender, R. 1989, A&A,, 215, 266
Nomoto, K., Thielemann, F. K., & Yokoi, K. 1984, ApJ, 286, 644
Peletier, R. F., Davies, R. L., Illingworth, G. D., Davis, L. E., & Cawson, M. 1990, AJ, 100, 1091
Pellegrini, S. 1994, A&A, in press
Pellegrini, S., & Fabbiano, G. 1994, ApJ, 429, 105
Renzini, A., Ciotti, L., D'Ercole, A., & Pellegrini, S. 1993, ApJ, 419, 52
Sage, L. J., & Wrobel, J. M. 1989, ApJ, 344, 204
Sandage, A. 1961, A Hubble Atlas of Galaxies (Washington: Carnegie Institute of Washington)
Sauvage, M., & Thuan, T. X. 1994, ApJ,, 429, 153
Schmitt, J. H. M. M. 1985, ApJ, 293, 178
Schweizer, F., & Seitzer, P. 1992, AJ, 104, 1039
Schweizer, F., Seitzer, P., Faber, S. M., Burstein, D., Dalle, Ore, C. M., & Gonzalez, J. J. 1990, ApJ, 364, L33
Serlemitsos, P. J., Loewenstein, M., Mushotzky, R. F., Marshall, F. E., & Petre, R. 1993, ApJ, 413, 518
Sil'chenko, O. K. 1994, Astron. Rept., 38, 3
Smith, E. P., & Heckman, T. M. 1989, ApJ, 341, 658
Spitzer, L., Jr. 1954, ApJ, 120, 1
Stiavelli, M., & Matteucci, F. 1991, ApJ, 377, L79
Terlevich, R., Davies, R. L., Faber, S. M., & Burstein, D. 1981, MNRAS, 196, 381
Thronson, H. A., Jr., Tacconi, L., Kenney, J., Greenhouse, M. A., Margulis, M., Tacconi-Garman, L., & Young, J. S. 1989, ApJ, 344, 747
Trinchieri, G., & Fabbiano, G. 1985, ApJ, 296, 447
Trinchieri, G., Fabbiano, G., & Canizares, C. R. 1986, ApJ, 310, 637
Trinchieri, G., Kim, D.-W., Fabbiano, G., & Canizares, C. 1994, ApJ, 428, 555
van Speybroeck, L., Epstein, A., Forman, W., Giacconi, R., & Jones, C. 1979, ApJ, 234, L45
Walsh, D. E. P., Knapp, G. R., Wrobel, J. M., & Kim, D.-W. 1989, ApJ, 337, 209
White, R. E., III, & Sarazin, C. L. 1991, ApJ, 367, 476
Woosley, S. E., & Weaver, T. A. 1986, in IAU Colloq. 89, Radiation Hydrodynamics in Stars and Compact Objects, ed. D. Mihalas & K. H. Winkler (Berlin: Springer), 91
Worthey, G. 1993, ApJ, 409, 530
———. 1994, ApJS, 95, 107
Worthey, G., Faber, S. M., & Gonzalez, J. J. 1992, ApJ, 398, 69
Wyse, R., & Silk, J. 1985, ApJ, 296, L1